Grand Asian Journal of Engineering and Advance Materials (GAJEAM)

Design and Numerical Formulation of Metamaterial Sensor for Evaluation of Dielectric Properties of the Materials

Dr. Abdul Samad[1], *Shahzaib*[1], *Khateeb Ahmad**[1],

[1] Department of Electrical Engineering, The University of Lahore Pakistan

Received data: 10 June 2025 Revised date: 15 July 2025 Accepted date: 21 July 2025 Published date: 1 August 2025

Abstract: Metamaterial-based microwave sensor with novel and compact resonator and slotted microstrip transmission line is proposed for efficient measurement of dielectric properties of the materials under test (MUTs). The proposed sensor is designed and simulated on commercially available substrate FR4 by using the ANSYS HFSS Software. A deep notch at -17 dB in the transmission coefficient (S21) is achieved at the resonant frequency of 3.88 GHz. The negative constitutive effective parameters (permittivity and permeability) are extracted from the S-parameters, which is the basic property of metamaterials or left-handed materials (LHMs). The sensitivity analysis is performed by placing various standard materials onto the sensor and measuring the shift in the resonant frequency of the MUTs. A parabolic equation of the proposed sensor is formulated to approximate the resonant frequency and the relative permittivity of the MUTs. A very strong agreement between the simulated and calculated results is found, which reveals that the proposed sensor is very efficient for the measurement of dielectric properties of the MUTs. Error analysis is performed to determine the accuracy of the proposed sensor. A very small percentage of error (0.31) is obtained, which indicates the high accuracy of the proposed sensor.

Keywords: Metamaterial sensor, Dielectric characterization, Relative permittivity, ANSYS HFSS simulation, Parabolic equation modeling

1. Introduction

Since the invention of metamaterials or left handed materials (LHMs), having unnatural and unique properties of the negative constitutive parameters (Smith, Padilla, Vier, Nemat-Nasser, & Schultz, 2000)(Veselago, 1967), the researchers and industries have produced numerous improved devices for the broad applications in the frequency range from RF to THz. Metamaterials are classified into two broad groups in which one is the split ring resonator (SRR), introduced by Pendry et. al. (Pendry, Holden, Robbins, & Stewart, 1999) and second is the complementary SRR (CSRR), introduced by Falcon et. al. (Falcone et al., 2004) as an effective negative permittivity particle.

In recent years, complementary metamaterial sensors (CSRR) are widely used in evaluation of dielectric substrate (Alimenti et al., 2023; Armghan, Alanazi, Altaf, & Haq, 2021; Cao, Ruan, Chen, & Zhang, 2022; Haq, Ruan, Zhang, & Ullah, 2019; Saadat-Safa, Nayyeri, Khanjarian, Soleimani, & Ramahi, 2019; Shahzad et al., 2022; Xiao, Yan, Guo,

& Chen, 2022), varactor-based tuneable metamaterial sensors (Shahzad, Hu, Ali, Barket, & Shah, 2024) dielectric characterization of ethanol-water mixture (Chuma, Iano, Fontgalland, & Roger, 2018; Zhang, Ruan, Haq, & Chen, 2019), testing of oil (Qureshi et al., 2021; Su, Mata-Contreras, Vélez, Fernández-Prieto, & Martín, 2018; Tiwari, Singh, & Akhtar, 2018; Zhang, Ruan, & Cao, 2022), measurement of thickness and permittivity (Lee & Yang, 2013, 2014), THz Antenna design (Esfandiyari et al., 2022), healthcare (Kumari, Patel, & Yadav, 2018), agriculture (Trabelsi & Nelson, 2016), organic tissues analysis (Puentes, Maasch, Schubler, & Jakoby, 2012) and environment (Abdolrazzaghi, Khan, & Daneshmand, 2018). The fundamental principle of microwave complementary metamaterial sensor is to sense the variation in resonance frequency and notch depth due to volume or permittivity perturbation of the MUTs. The key advantages of metamaterial-based microwave sensors are high sensitivity, inexpensive fabrication, robust design, and integration with other microwave components. According to (Baena et al., 2005), complementary metamaterial resonators exhibits cross polarization effects, which implies that these resonators can show electric and magnetic dipole resonance if properly excited by external electric and magnetic fields respectively.

Permittivity is one of the important parameters to analyse the behaviour of the materials. For the development of the sophisticated microwave devices, prior knowledge of the materials' permittivity is essential. There are four types of approaches classified for the characterization of the materials including free space, transmission line, near field and resonance-based [27]. Among them the resonance-based approach is implemented in the presented work which is economical, efficient and highly precise for the measurement of dielectric properties of the MUTs. Particularly, the use of complementary metamaterial sensor for the measurement of dielectric properties of the MUTs is very convenient since the capacitance (and hence the resonant frequency) is very sensitive to the presence of the MUT onto the sensor. The variation of the sensing stimuli modifies the resonant properties of the sensor like notch frequency, *Q*-factor, and notch depth during the interaction (Vivek, Shambavi, & Alex, 2019)

On the basis of measured data, dielectric properties of various MUTs can be estimated.

In literature, metamaterial-based microwave sensors have been reported operating at single (Mohammad Arif Hussain Ansari, Jha, & Akhtar, 2015; Muhammed Said Boybay & Ramahi, 2012; Muhammed S Boybay & Ramahi, 2013; Ebrahimi, Withayachumnankul, Al-Sarawi, & Abbott, 2013), dual (Lee & Yang, 2015; Su, Mata-Contreras, Velez, & Martín, 2016), triple (Yang, Lee, Chen, & Chen, 2015) and tetra frequency bands (M Arif Hussain Ansari, Jha, Akhter, & Akhtar, 2018). The metamaterial sensors reported in the literature have some limitations regarding sensitivity, measurement range, efficiency and accuracy. In this work, a highly sensitive metamaterial-based microwave sensor is proposed for efficient characterization of dielectric properties of the MUTs. The sensitivity limitations, measuring range and accuracy issues experienced in the previously reported metamaterial sensors are overcome in this work by designing a high frequency resonator and slotted microstrip transmission line. The equivalent circuit model of the proposed sensor is developed that describes the overall behavior of the sensor.

2. Design and Parametric Analysis

The proposed sensor is designed on commercially available substrate FR4 on using the ANSYS HFSS. The thickness of the substrate is optimized to 1 mm, whereas the length and the width of the substrate are 30 mm and 24 mm respectively. On the one layer of the substrate (top layer), a slotted microstrip

transmission line is printed. The size of the microstrip line is optimized as length=30 mm, width=1.9 mm and thickness=0.017 mm to achieve the characteristics impedance of 50 Ω by using the expression of the microstrip transmission line (Hong & Lancaster, 2004). The length of the slots at microstrip line is 4mm whereas the dimensions of other design parameters *a*, *b*, *c*, *d*, and *e* is 0.38 mm shown (Fig. 1*a*).

Second layer (ground layer) of the substrate is coated with copper having thickness 0.017 mm.

The proposed CSRR resonator is etched from the copper layer in the ground layer as shown (Fig. 1b). The dimension of design parameters of the proposed resonator m, n, o, p, and g is 0.3 mm. All the dimensions in this work are taken in the mm scale.

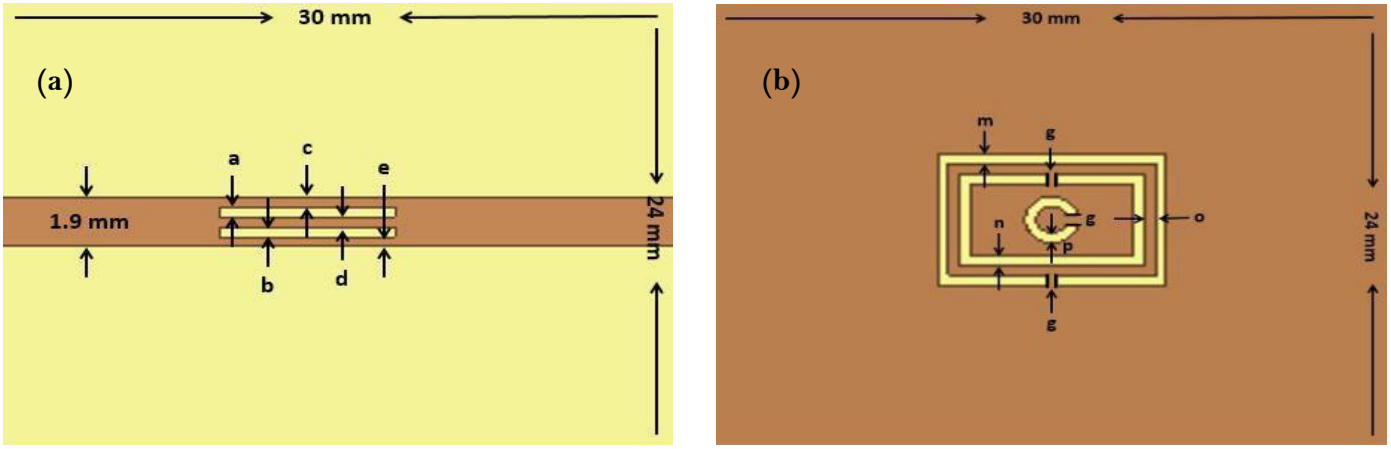

Fig. 1 ***Lay-out of the proposed sensor,*** **Slotted microstrip line,** ***(b)*** **Proposed CSRR resonator**

The slotted microstrip transmission line is introduced in this work to enhance the sensitivity of the proposed sensor. The slots in the microstrip line are used to increase the flux concentration which in turn increases the electric fringing field. The sensitivity of the sensor increases with the increase in the electric fringing fields. The effect of microstrip line parameters is analyzed on the resonant characteristics of the proposed sensor on using the ANSYS HFSS. The parameters *a* and *b* represent the capacitive elements, whereas *c*, *d*, and *e* represent the inductive elements. By increasing *a* and *b* one by one, the effective capacitance of the sensor decreases which in turn increases the resonant frequency (*fr*) of the sensor according to the equation (1). Contrarily, by increasing *c*, *d* and *e* one by one, the copper area around the slots increases which in turn decreases the inductance of the sensor. By decreasing in the inductance, the resonant frequency of the sensor increases accordingly. Graphical representation of the effects of the design parameters of the microstrip line on the resonant characteristics of the sensor

are shown (Fig. 2*a*).

The resonant characteristics of the sensor can also be controlled by varying the design parameters of the resonator (*m*, *n*, *o*, *p*, and *g*). The parameter *m* and *n* designate the outer and inner rectangle, respectively, which represent the capacitive element. The parameters *o* and *g* designate the thickness between the rectangles and the slits respectively, which represent the inductive element of the sensor. By increasing the parameters *m* and *n* one by one,

the effective capacitance decreases which in turn increases the resonant frequency (f_r) of the sensor. However, increasing the parameter p, the copper area of the inner ring of the resonator reduces. Keeping in view the cylindrical geometry, inner radius of the cylinder decreases which in turn increases the overall inductance of the sensor. As an increase in the inductance, the resonant frequency (f_r) of the sensor decreases. Graphical representation of the effects of design parameters of the resonator on the resonant characteristics are shown (Fig. 2*b*).

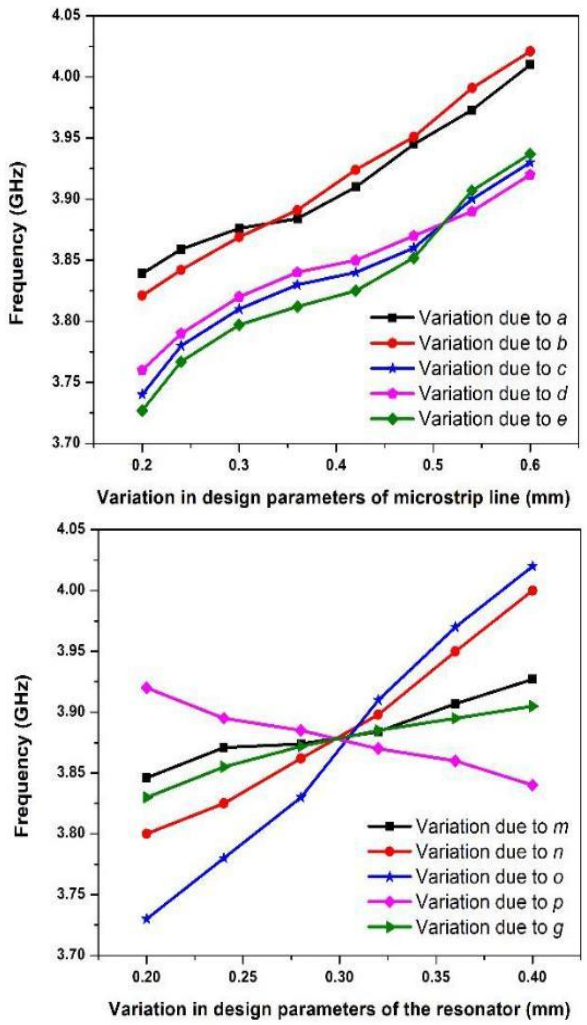

Fig. 2 Effect of design parameters of the microstrip line and resonator on the resonant characteristic of the sensor (a) Variation in design parameters of the microstrip line, (b) Variation in design parameters of the resonator

Keeping in view the sensitivity and accuracy of the sensor, parametrical and geometrical measures of the proposed sensor are chosen after numerous iterative simulations such that the sensitivity and accuracy may be improved for the precise measurement as compared to the metamaterial sensors reported in literature.

The overall behavior of the proposed sensor can be analyzed by its lumped elements equivalent circuit model as shown (Fig. 3). The equivalent circuit model is developed on using the NI Multisim

software. The resonance structure of the sensor consists of two parts: first is the slotted microstrip line with a coupling capacitance represented by the symbol C. Second is the resonator layer, which has a variable capacitance represented by the symbol Cc. These two parts provide with the two shunt capacitance values that form the total capacitance of the sensor. The symbols *Lc* and *Rc* represent the inductance and resistance of the unit cell, respectively. The resistance *Rc* accounting for the losses in the unit cell, whereas the parallel combination of the two inductances labelled with the symbol *L/2* represents the line inductance. By optimizing the design parameters of the slotted microstrip line and resonator, performance of the proposed sensor can be controlled effectively. The expression for the proposed sensor can be modelled by RLC circuit whose resonant frequency (*fr*) is given by (Muhammed Said Boybay & Ramahi, 2012).

$$f_r = \frac{1}{2\pi\sqrt{L_c(C+C_c)}} \quad (1)$$

The resonant frequency (*fr*) of the resonator, couple with the microstrip line, is the function of three parameters (*Lc, C, Cc*). With the change in the inductance and capacitance due to interaction with the MUTs, the resonant frequency of the sensor changes accordingly.

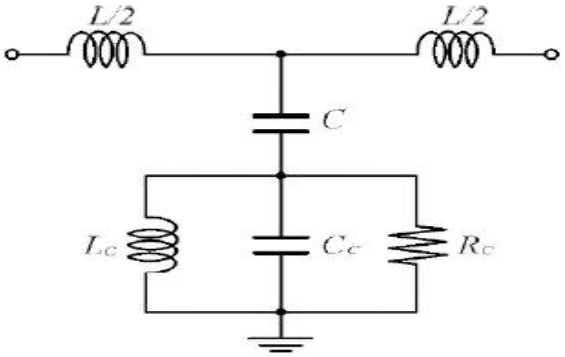

Fig. 3 Lumped element equivalent circuit model

3. Simulations and Performance Analysis

The proposed sensor is designed and simulated on using the ANSYS HFSS. Magnitude of S-parameters i-e reflection coefficient (*S11*) and transmission coefficient (*S21*) of the proposed sensor are shown (Fig. 4). A deep notch at - 17 dB is achieved in the transmission coefficient (*S21*) at the resonant frequency of 3.88 GHz as shown (Fig. 4). The constitutive effective parameters i-e permittivity (εr) and permeability (μr) of the proposed sensor are retrieved from the S-parameters data. By properly coupling the CSRR resonator to a host microstrip line, the structure with the negative constitutive parameters can be achieved. An effective negative valued permeability can be obtained by periodically etching the capacitive gaps in the conductor strip at periodic position (Baena et al., 2005).

The graph of effective permittivity and permeability are shown (Fig. 5). Both the effective permittivity and permeability are negative at the vicinity of the resonant frequency of the sensor. The permittivity is negative from 3.82 GHz to 4.35 GHz whereas the permeability is negative from 3.72 GHz to 3.83 GHz. Both the constitutive parameters are negative, which describe the basic property of a metamaterial/LHM.

The effective permittivity and permeability of the metamaterial sensor can be retrieved from its transmission (S21) and reflection (S11) coefficients

using the following expressions (Chen, Grzegorczyk, Wu, Pacheco Jr, & Kong, 2004).

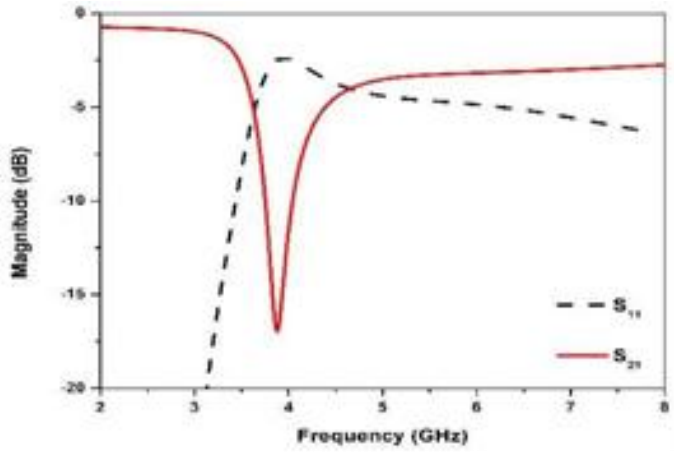

Fig. 4 Magnitude of S-parameters of the proposed sensor

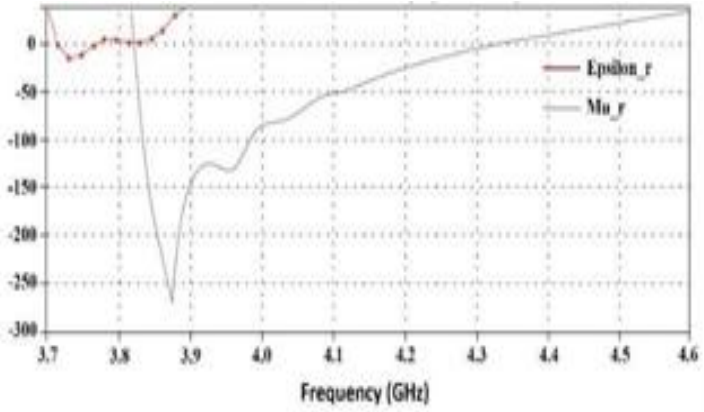

Fig.5 Extracted plots of the negative permittivity and permeability of the proposed sensor

$$S_{11} = \frac{R_{01}(1-e^{i2nkod})}{1-R_{01}^2 e^{i2nkod}} \quad (2)$$

$$S_{21} = \frac{(1-R_{01}^2)e^{inkod}}{1-R_{01}^2 e^{i2nkod}} \quad (3)$$

Since $R_{01}=z-1/z+1$

Where n is the refractive index, z is the impedance, $k0$ is the wave number of the incident wave in free space, d is the thickness of material/slab. The refractive index (n) and the impedance (z) are obtained by inverting the equation (2) and (3), yielding;

$$z = \pm\left\{\sqrt{\frac{(1+S_{11})^2-S_{21}^2}{(1-S_{11})^2-S_{21}^2}}\right\} \quad (4)$$

$$Q = e^{inkod} = \frac{S_{21}}{1-S_{11}(z-1/z+1)} \quad (5)$$

$$n = \frac{1}{k_0 d}\left[\{Im[In(Q)] + 2m\pi\} - i.R_e[In(Q)]\right] \quad (6)$$

Both the effective permittivity (ε) and permeability (μ) are associated with the refractive index (n) and the impedance ($\approx$) as;

$$\varepsilon = n / z \quad (7)$$

$$\mu = nz \quad (8)$$

The electric and magnetic field distributions around the resonator are investigated through the ANSYS HFSS. The concentration of the electric and magnetic fields is shown (Fig. 6a) and (Fig. 6b) respectively. The maximum electric field concentration around the resonator is 2.59 x 10^4 V/m, and the magnetic field concentration is 1.64 x 10^2 A/m. When a MUT is placed onto the resonator for the characterization, then the electric and magnetic field get perturbed. This perturbation of the electric and magnetic fields leads to change in the resonant frequency of the sensor. To map the change in the resonant frequencies with the permittivity of the MUT, a numerical model for the proposed sensor is developed to approximate the permittivity of the MUTs.

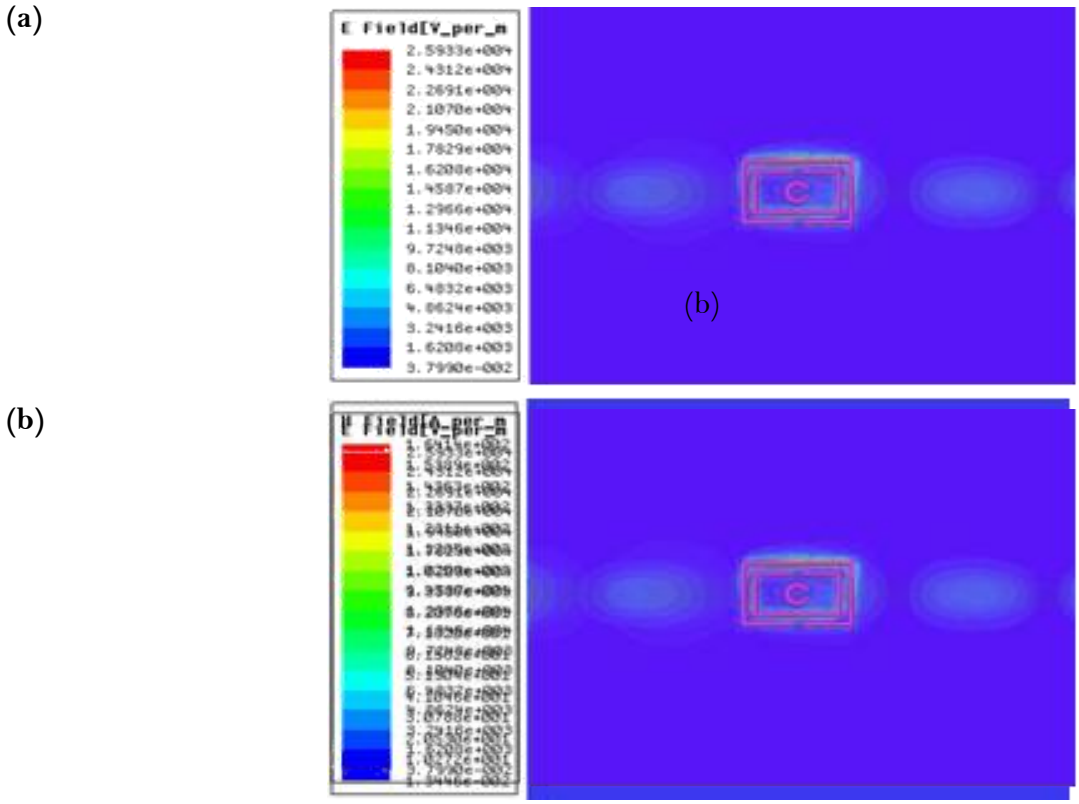

Fig. 6 Concentration of electric and magnetic fields; Electric fields concentration of the sensor, (b) Magnetic fields concentration of the sensor

4. Numerical Simulations

From the theory of perturbation, when a MUT is placed onto the sensor, it interacts with the electric and magnetic fields of the sensor and perturbs the field distribution. Consequently, phenomena of shift in the resonant frequency occur. The relation between the resonant frequency of a microwave sensor and the dielectric properties of the MUTs can be described numerically as (Chen et al., 2004).

$$\frac{\Delta f_r}{f_r} = \frac{\int_v (\Delta\epsilon E_1 . E_0 + \Delta\mu H_1 . H_0) dv}{\int_v (\varepsilon_0 |E_0|^2 + \mu_0 |H_0|^2) dv} \quad (9)$$

Here, Δfr is the shift in the resonant frequency (fr) due to the interaction with the MUTs. $\varepsilon 0$ and $\mu 0$ are the permittivity and permeability of the free space while $\Delta\varepsilon$ and $\Delta\mu$ are the change in the permittivity and permeability, respectively. $E0$ and $H0$ are the electric and magnetic fields before the interaction with the MUTs, whereas $E1$ and $H1$ are the perturbed fields and v is the perturbed volume. If the intensity of the magnetic field is higher than that of the electric field, the phenomenon of the shift in the resonant frequency occurs due to the permeability of the MUT. Contrarily, if the intensity of the electric field is higher, the shift in the resonant frequency happens due to the permittivity of the MUT. In the present work, the intensity of the electric field is higher than that of the magnetic field; hence, the phenomenon of the shift in the resonant frequency occurs due to the interaction with the permittivity of the MUT.

The sensitivity analysis is performed using the proposed sensor through the ANSYS HFSS. The shift in the resonant frequency of the proposed sensor is measured under both the loaded and unloaded conditions. The standard MUTs including Rogers 5880, Rogers 3003, Plexiglass, Rogers TMM, Quartz glass and FR4 are used in the present work for the sensitivity analysis. These MUTs with the same dimensions (7 mm x 5mm x 1 mm) are placed one by one onto the resonator in the ground plane of the proposed sensor without air gap as shown (Fig. 7) and measuring the shift in the resonant frequency of the sensor due to interaction with these MUTs, which is shown graphically (Fig. 8). By increasing the permittivity of the MUT, the resonant frequency of the sensor decreases accordingly. The shift in the resonant frequency corresponding to every value of the permittivity of the MUTs is recorded and tabulated in Table 1.

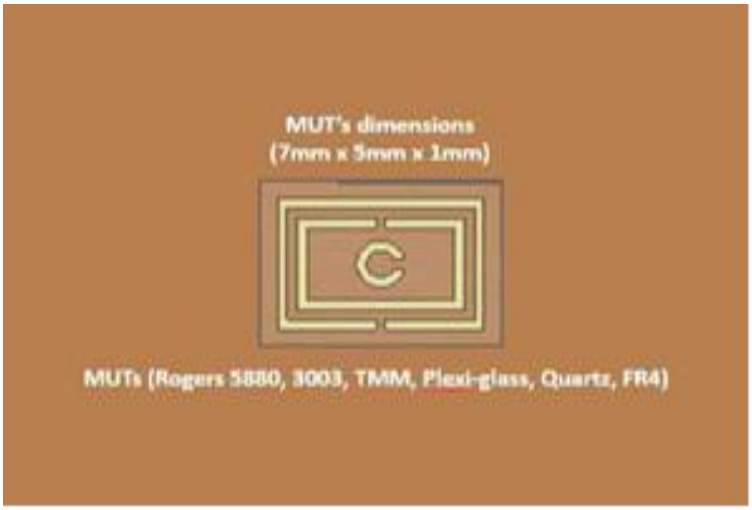

Fig. 7 Dimension and position of the MUTs in the ground plane of the proposed sensor

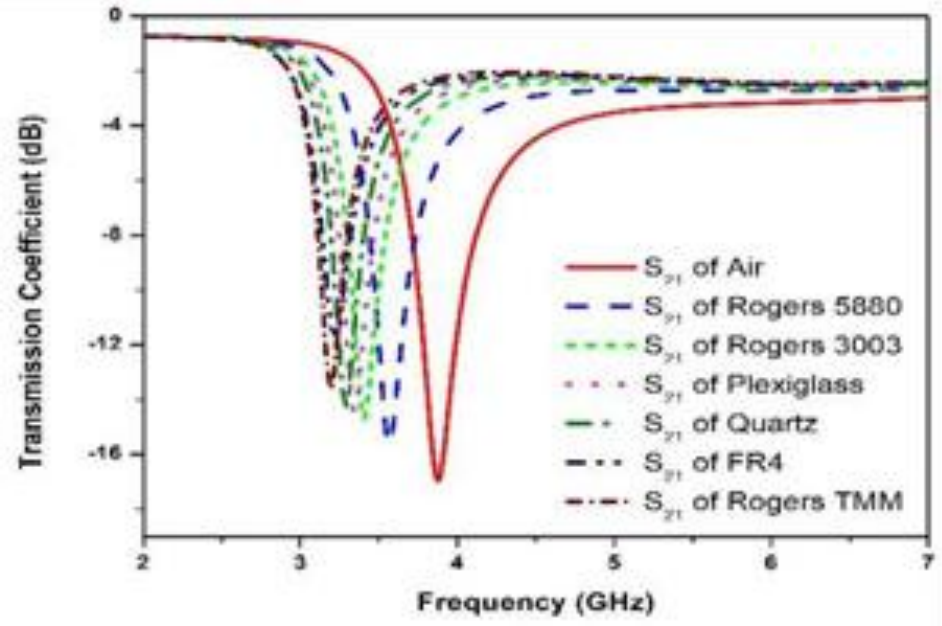

Fig. 8 Shift in the resonant frequency of the proposed sensor due to interaction with the MUTs

Table 1 Shift in the resonant frequency of the sensor due to interaction with the MUTs

MUTs	Permittivity (εr)	Simulated Frequency (GHz)
Air	1	3.88
Rogers (5880)	2.2	3.57
Rogers (3003)	3	3.41
Plexiglass	3.4	3.34
Quartz	3.78	3.28
FR4	4.4	3.21

Basically, when a MUT is placed onto the resonator, it perturbs the field distributions during the interaction. Consequently, the capacitance of the sensor increases which in turn decreases the resonant frequency as discussed in equation (1).

5. Equation Formulation

The parabolic equation of the proposed sensor with fitting parameters is formulated for the approximation of the relative permittivity of the materials under test (MUTs). The parabolic equation is fairly reliable to approximate the relative permittivity of the materials ranging up to 10. The

parabolic equation can be expressed as (Lim, Kim, & Hong, 2018);

$$f_{r,MUT} = A_1 + A_2(\varepsilon_{r,MUT}) + A_3(\varepsilon_{r,MUT})^2 \quad (10)$$

Here, fr,MUT and $\varepsilon r,MUT$ are the resonant frequency and the relative permittivity of the MUT, respectively. $A1$, $A2$ and $A3$ are the constants of polynomial. In this analysis, air is the reference MUT having permittivity equal to 1 approximately. Hence, the parabolic equation (10) can further be expanded with respect to the permittivity of the reference MUT as;

$$f_{r,MUT} = A_1 + A_2(\varepsilon_{r,MUT} - 1) + A_3(\varepsilon_{r,MUT} - 1)^2 \quad (11)$$

The constant parameters $A1$, $A2$, and $A3$ are calculated by inserting the simulated values of the standard MUTs (Air, Rogers 5880, and Plexiglass) from Table 1. After simplifications, the parabolic equation for the proposed sensor can be expressed as;

$$f_{r,MUT} = 3.88 - 0.2916(\varepsilon_r - 1) + 0.0277(\varepsilon_r - 1)^2 \quad (12)$$

The resonant frequency of a material can be estimated from the equation (12) by inserting the value of relative permittivity ($\varepsilon r,MUT$) of that material. The resonant frequency of the standard materials, used in this work, are calculated by inserting their values of real permittivity ($\varepsilon r,MUT$) in the equation (12), and the results are tabulated in Table 2. The calculated response is found very close to the simulated response, which shows strong agreement between them. Error analysis is performed on the simulated and calculated resonant frequencies to determine the accuracy. A very small percentage of error (% error) is achieved (Table 2), which indicates high accuracy of the proposed sensor.

Table 2 Comparison of simulated and calculated response in terms of frequency (fr) and error analysis

MUTs	Permittivity (εr)	Simulated (GHz)	Calculated (GHz)	% Error
Air	1	3.88	3.88	0.00
Rogers (5880)	2.2	3.57	3.567	0.08
Rogers (3003)	3	3.41	3.407	0.08
Plexi Glass	3.4	3.34	3.339	0.03
Quartz Glass	3.78	3.28	3.283	0.09
FR4	4.4	3.21	3.208	0.06
Rogers, TMM	4.5	3.2	3.199	0.03

The parabolic equation (12) is further simplified to estimate the relative permittivity of the MUT, which can be expressed as;

$$\varepsilon_r = \frac{0.2916-\sqrt{(0.085-0.1108(3.88-f_r)}}{0.0554} + 1 \quad (13)$$

Table 3 Comparison of simulated and calculated response in terms of permittivity (εr) and error analysis

MUTs	Frequency (GHz)	Real Permittivity	Calculated Permittivity	% Error
Air	3.88	1	1.001	0.1
Rogers (5880)	3.57	2.2	2.21	0.4
Rogers (3003)	3.41	3	2.98	0.6
Plexi Glass	3.34	3.4	3.39	0.2
Quartz Glass	3.28	3.78	3.80	0.5
FR4	3.21	4.4	4.39	0.2
Rogers, TMM	3.20	4.5	4.49	0.2

The relative permittivity (εr,*MUT*) of any MUT can be approximated from the equation (13) by inserting the resonant frequency (*fr*,*MUT*) of the corresponding MUT. The relative permittivity of the standard MUTs, used in this work, is also evaluated by inserting their simulated resonant frequencies (*fr*,*MUT*), mentioned in Table 1, in the formulated equation (13). The calculated values of the relative permittivity of the standard MUTs are tabulated in Table 3. There is a negligible difference between the real and calculated permittivity of the MUTs. Error analysis is carried-out on the real and calculated permittivity of the MUTs. A very small percentage of error (% error) is obtained as shown in Table 3, which reveals high accuracy of the proposed sensor.

6. Results and Discussions

The proposed sensor is used to measure the shift in the resonant frequency of the sensor due to the interaction with the MUTs and to approximate the relative permittivity of the corresponding MUTs using the formulated parabolic equation. In the present work, various standard MUTs including Rogers 5880, 3003, TMM, Plexiglass, Quartz and FR4 are used for the sensitivity analysis. The simulation is performed using the proposed sensor by placing these standard materials and measuring the shift in the resonant frequency of the sensor. A strong agreement between the results is found and a very small percentage of error (% error) is achieved which indicate high accuracy of the proposed sensor.

The resonant frequency of the standard materials is calculated by using the formulated parabolic equation (12) of the proposed sensor, tabulated the

results in Table 2. The performance comparison between the simulated and calculated results in terms of the resonant frequency is carried-out and illustrated graphically, as shown (Fig. 9). Both the curves are in the strong agreement due to negligible difference between them. The achieved results reveal high accuracy of the proposed sensor.

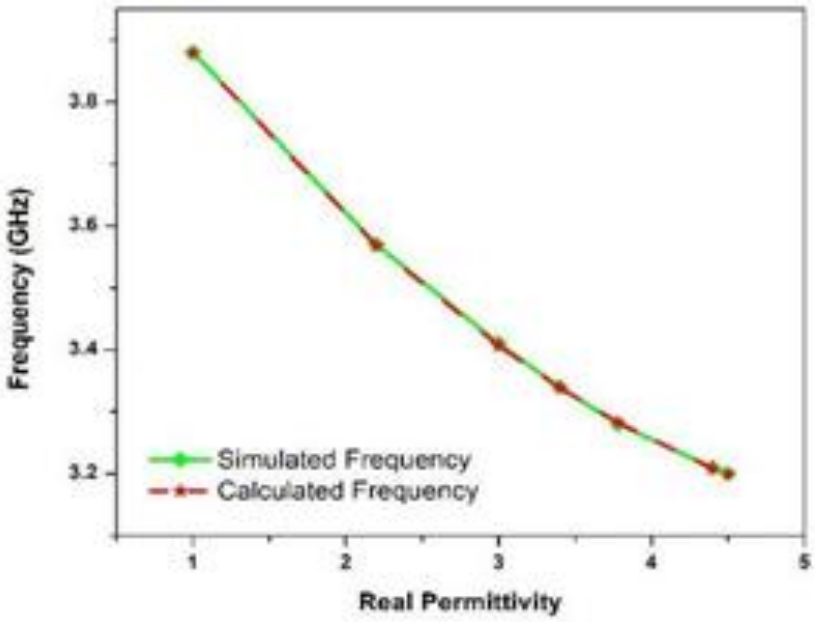

Fig. 9 Graphical representation of comparison of simulated and calculated resonant frequencies

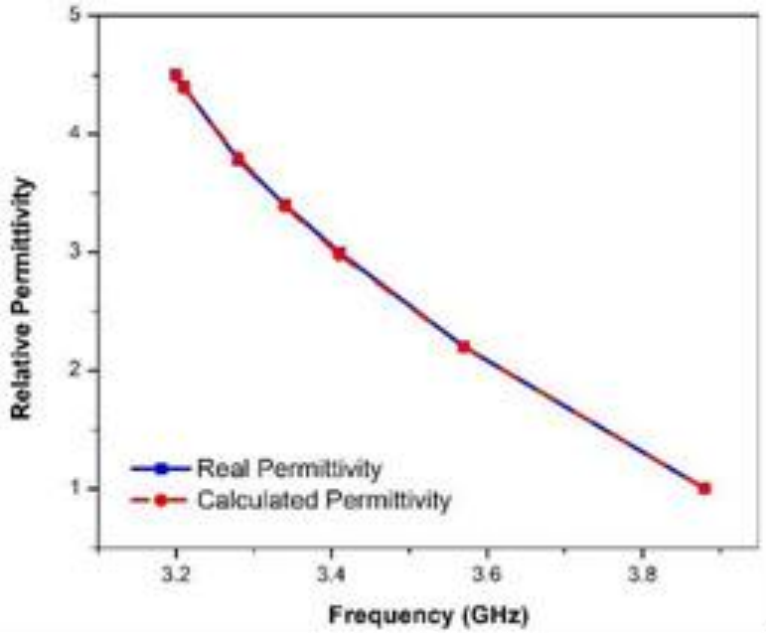

Fig. 10 Graphical representation of comparison of real and calculated permittivity

Table 4 Performance analysis between the proposed sensor and the sensors reported in literature

Sensor Range	Frequency (GHz)	Mean % Error
≈ 2.3	2.65	2.28
≈ 10	2.7	3.43
≈ 6	1.7	1.96
≈ 5.8	3	1.81
≈ 6.5	2.1	3.4
≈ 8	2.41	3.73
≈ 6.7	2.74	4.62
≈ 5.8	2.45	2.84

The sensor is proposed for the measurement of the relative permittivity of the materials under test. The relative permittivity of the standard materials is calculated by using the formulated parabolic equation (13), and tabulated the results in Table 3. The performance analysis between the simulated and calculated results in terms of permittivity is carried-out and illustrated graphically, as shown (Fig. 10).

Both the curves are found very close, which show a very strong agreement between them and high accuracy of the proposed sensor.

Comparative analysis in terms of the overall performance is executed between the proposed sensor and the sensors reported in literature, which is shown in Table 4. The overall performance of the proposed sensor is better than the other reported sensors. A very small percentage of error

(0.31) is achieved, which is the lowest as compared to the previously reported work. The sensitivity and accuracy of the proposed sensor are much better than that of the metamaterial sensors reported in literature.

7. Conclusion

A highly accurate complementary metamaterial sensor was proposed for the precise measurement of the relative permittivity of the materials under test. The proposed sensor was designed and simulated on commercially available substrate FR4 on using the

simulation software ANSYS HFSS. The sensitivity of the proposed sensor was improved by introducing slotted microstrip transmission line. A deep notch at -17 dB is achieved at the resonant frequency of 3.88 GHz. The negative constitutive parameters (permittivity and permeability) were retrieved from the S-parameters, which is the basic property of metamaterial or LHM. The sensitivity analysis was performed by placing various standard material onto the proposed sensor. A parabolic equation was formulated to approximate the relative permittivity of the materials under test. A very strong agreement was achieved between the simulated and calculated results. Error analysis was performed to determine the accuracy of the proposed sensor. A very small percentage of error (0.31) was achieved, which reveals high accuracy of the proposed sensor. Although the sensitivity analysis is carried-out through the proposed sensor by placing materials in solid format, but the proposed sensor can equally be used for the efficient characterization of the MUTs in powder format. The proposed sensor is very compact and robust that will be used for bio-sensing, liquid determination and security applications in the future.

Data Availability: The data used to support the findings of this study are available from the corresponding author upon request.

Conflicts of Interest: The authors declare that there is no conflict of interest regarding the publication of this paper.

References

Abdolrazzaghi, M., Khan, S., & Daneshmand, M. (2018). A dual-mode split-ring resonator to eliminate relative humidity impact. *IEEE microwave and wireless components letters*, *28*(10), 939-941.

Alimenti, A., Pittella, E., Torokhtii, K., Pompeo, N., Piuzzi, E., & Silva, E. (2023). A dielectric loaded resonator for the measurement of the complex permittivity of dielectric substrates. *IEEE Transactions on Instrumentation and Measurement*, *72*, 1-9.

Ansari, M. A. H., Jha, A. K., & Akhtar, M. J. (2015). Design and application of the CSRR-based planar sensor for noninvasive measurement of complex permittivity. *IEEE Sensors Journal*, *15*(12), 7181-7189.

Ansari, M. A. H., Jha, A. K., Akhter, Z., & Akhtar, M. J. (2018). Multi-band RF planar sensor using complementary split ring resonator for testing of dielectric materials. *IEEE Sensors Journal*, *18*(16), 6596-6606.

Armghan, A., Alanazi, T. M., Altaf, A., & Haq, T. (2021). Characterization of dielectric substrates using dual band microwave sensor. *IEEE Access*, *9*, 62779-62787.

Baena, J. D., Bonache, J., Martín, F., Sillero, R. M., Falcone, F., Lopetegi, T., . . . Portillo, M. F. (2005). Equivalent-circuit models for split-ring resonators and complementary split-ring resonators coupled to planar transmission lines. *IEEE transactions on microwave theory and techniques*, *53*(4), 1451-1461.

Boybay, M. S., & Ramahi, O. M. (2012). Material characterization using complementary split-ring resonators. *IEEE Transactions on Instrumentation and Measurement*, *61*(11), 3039-3046.

Boybay, M. S., & Ramahi, O. M. (2013). Non-destructive thickness measurement using quasi-static resonators. *IEEE microwave and wireless components letters*, *23*(4), 217-219.

Cao, Y., Ruan, C., Chen, K., & Zhang, X. (2022). Research on a high-sensitivity asymmetric metamaterial structure and its application as microwave sensor. *Scientific Reports*, *12*(1), 1255.

Chen, X., Grzegorczyk, T. M., Wu, B.-I., Pacheco Jr, J., & Kong, J. A. (2004). Robust method to retrieve the constitutive effective parameters of metamaterials. *Physical Review E—Statistical, Nonlinear, and Soft Matter Physics*, *70*(1), 016608.

Chuma, E. L., Iano, Y., Fontgalland, G., & Roger, L. L. B. (2018). Microwave sensor for liquid dielectric characterization based on metamaterial complementary split ring resonator. *IEEE Sensors Journal*, *18*(24), 9978-9983.

Ebrahimi, A., Withayachumnankul, W., Al-Sarawi, S., & Abbott, D. (2013). High-sensitivity metamaterial-inspired sensor for microfluidic dielectric characterization. *IEEE Sensors Journal*, *14*(5), 1345-1351.

Esfandiyari, M., Lalbakhsh, A., Jarchi, S., Ghaffari-Miab, M., Mahtaj, H. N., & Simorangkir, R. B. (2022). Tunable terahertz filter/antenna-sensor using graphene-based metamaterials. *Materials & Design*, *220*, 110855.

Falcone, F., Lopetegi, T., Baena, J. D., Marqués, R., Martín, F., & Sorolla, M. (2004). Effective negative-/spl epsiv/stopband microstrip lines based on complementary split ring resonators. *IEEE microwave and wireless components letters*, *14*(6), 280-282.

Haq, T. u., Ruan, C., Zhang, X., & Ullah, S. (2019). Complementary metamaterial sensor for nondestructive evaluation of dielectric substrates. *Sensors*, *19*(9), 2100.

Hong, J.-S. G., & Lancaster, M. J. (2004). *Microstrip filters for RF/microwave applications*: John Wiley & Sons.

Kumari, R., Patel, P. N., & Yadav, R. (2018). An ENG-inspired microwave sensor and functional technique for label-free detection of aspergillus Niger. *IEEE Sensors Journal*, *18*(10), 3932-3939.

Lee, C.-S., & Yang, C.-L. (2013). Thickness and permittivity measurement in multi-layered dielectric structures using complementary split-ring resonators. *IEEE Sensors Journal*, *14*(3), 695-700.

Lee, C.-S., & Yang, C.-L. (2014). Complementary split-ring resonators for measuring dielectric constants and loss tangents. *IEEE microwave and wireless components letters*, *24*(8), 563-565.

Lee, C.-S., & Yang, C.-L. (2015). Single-compound complementary split-ring resonator for simultaneously measuring the permittivity and thickness of dual-layer dielectric materials. *IEEE transactions on microwave theory and techniques*, *63*(6), 2010-2023.

Lim, S., Kim, C.-Y., & Hong, S. (2018). Simultaneous measurement of thickness and permittivity by means of the resonant frequency fitting of a microstrip line ring resonator. *IEEE microwave and wireless components letters*, *28*(6), 539-541.

Pendry, J. B., Holden, A. J., Robbins, D. J., & Stewart, W. J. (1999). Magnetism from conductors and enhanced nonlinear phenomena. *IEEE transactions on microwave theory and techniques*, *47*(11), 2075-2084.

Puentes, M., Maasch, M., Schubler, M., & Jakoby, R. (2012). Frequency multiplexed 2-dimensional sensor array based on split-ring resonators for organic tissue analysis. *IEEE transactions on microwave theory and techniques*, *60*(6), 1720-1727.

Qureshi, S. A., Zainal Abidin, Z., Isa Ashyap, A. Y., Majid, H. A., Kamarudin, M. R., Yue, M., . . . Nebhen, J. (2021). Millimetre-wave metamaterial-based sensor for characterisation of cooking oils. *International Journal of Antennas and Propagation*, *2021*(1), 5520268.

Saadat-Safa, M., Nayyeri, V., Khanjarian, M., Soleimani, M., & Ramahi, O. M. (2019). A CSRR-based sensor for full characterization of magneto-dielectric materials. *IEEE transactions on microwave theory and techniques*, *67*(2), 806-814.

Shahzad, W., Hu, W., Ali, Q., Barket, A. R., & Shah, G. (2024). Varactor-Based Tunable Sensor for Dielectric Measurements of Solid and Liquid Materials. *Journal of Sensor and Actuator Networks*, *13*(1), 8.

Shahzad, W., Hu, W., Ali, Q., Raza, H., Abbas, S. M., & Ligthart, L. P. (2022). A Low-cost metamaterial sensor based on DS-CSRR for material characterization applications. *Sensors*, *22*(5), 2000.

Smith, D. R., Padilla, W. J., Vier, D. C., Nemat-Nasser, S. C., & Schultz, S. (2000). Composite medium with simultaneously negative permeability and permittivity. *Physical review letters*, *84*(18), 4184.

Su, L., Mata-Contreras, J., Vélez, P., Fernández-Prieto, A., & Martín, F. (2018). Analytical method to estimate the complex permittivity of oil samples. *Sensors*, *18*(4), 984.

Su, L., Mata-Contreras, J., Velez, P., & Martín, F. (2016). Splitter/combiner microstrip sections loaded with pairs of complementary split ring resonators (CSRRs): Modeling and optimization for differential sensing applications. *IEEE transactions on microwave theory and techniques*, *64*(12), 4362-4370.

Tiwari, N. K., Singh, S. P., & Akhtar, M. J. (2018). Novel improved sensitivity planar microwave probe for adulteration detection in edible oils. *IEEE microwave and wireless components letters*, *29*(2), 164-166.

Trabelsi, S., & Nelson, S. O. (2016). Microwave sensing of quality attributes of agricultural and food products. *IEEE instrumentation & measurement magazine*, *19*(1), 36-41.

Veselago, V. (1967). The electrodynamics of substances with simultaneously negative values of and. *Usp. fiz. nauk*, *92*(3), 517-526.

Vivek, A., Shambavi, K., & Alex, Z. C. (2019). A review: metamaterial sensors for material characterization. *Sensor Review*, *39*(3), 417-432.

Xiao, H., Yan, S., Guo, C., & Chen, J. (2022). A dual-scale CSRRs-based sensor for dielectric characterization of solid materials. *IEEE Sensors Letters*, *6*(12), 1-4.

Yang, C.-L., Lee, C.-S., Chen, K.-W., & Chen, K.-Z. (2015). Noncontact measurement of complex permittivity and thickness by using planar resonators. *IEEE transactions on microwave theory and techniques*, *64*(1), 247-257.

Zhang, X., Ruan, C., & Cao, Y. (2022). A dual-mode microwave sensor for edible oil characterization using magnetic-LC Resonators. *Sensors and Actuators A: Physical*, *333*, 113275.

Zhang, X., Ruan, C., Haq, T. u., & Chen, K. (2019). High-sensitivity microwave sensor for liquid characterization using a complementary circular spiral resonator. *Sensors*, *19*(4), 787.